Novel carbon fiber composite for hip replacement with improved in vitro and in vivo osseointegration

Dimitrievska, Sashka; Whitfield, James; Hacking, Adam; Bureau, Martin

Publisher's version / Version de l'éditeur:
https://doi.org/10.1002/jbm.a.32175
Journal of Biomedical Materials Research Part A, 91A, August 1, pp. 37-51, 2008

Editorial Manager(tm) for Biomaterials
Manuscript Draft

Manuscript Number:

Title: Novel carbon fiber composite with bone matching stiffness for hip replacement with improved in vitro and in vivo osseointegration

Article Type: FLA Original Research

Section/Category: Biomaterials & Biocompatibility

Keywords: Hip replacement prosthesis; Composite; ECM (extracellular matrix); Osseointegration

Corresponding Author: Dr. Martin N. Bureau, PhD. , Eng.

Corresponding Author's Institution: National Research Council Canada

First Author: Sashka Dimitrievska, MSc

Order of Authors: Sashka Dimitrievska, MSc; James Whitfield, PhD; Adam Hacking, PhD; Martin N. Bureau, PhD. , Eng.

Manuscript Region of Origin:

Abstract: A novel composite femoral stem has been developed to match cortical stiffness and achieve fixation by osseointegration with the primary goal to reduce cortical bone loss associated with stress shielding. The femoral stem consists of three distinct material layers: the first is a long carbon fiber (CF) in a polyamide 12 (PA12) polymer matrix (PA12/CF); the second is a PA12/HA (hydroxyapatite) interface; and the third is a plasma-sprayed coating of HA. In vitro studies with MG63 cells indicated that the HA surface supported improved proliferation and differentiation of osteoblast-like cells as determined by alkaline phosphatase (ALP) activity and osteocalcin production when compared to Ti-6Al-4V (Ti64). In vivo studies comparing the composite and Ti64 rods in the rabbit femur demonstrated significantly higher bone apposition to the composite than Ti64 rods. The results of this study indicate that the invasion of surrounding

bone cells and thus osteointegration together with its bone-matching mechanical properties make the PA12/CF/HA stem an interesting hip replacement candidate.

ABSTRACT

A novel composite femoral stem has been developed to match cortical stiffness and achieve fixation by osseointegration with the primary goal to reduce cortical bone loss associated with stress shielding. The femoral stem consists of three distinct material layers: the first is a long carbon fiber (CF) in a polyamide 12 (PA12) polymer matrix (PA12/CF); the second is a PA12/HA (hydroxyapatite) interface; and the third is a plasma-sprayed coating of HA. *In vitro* studies with MG63 cells indicated that the HA surface supported improved proliferation and differentiation of osteoblast-like cells as determined by alkaline phosphatase (ALP) activity and osteocalcin production when compared to Ti-6Al-4V (Ti64). *In vivo* studies comparing the composite and Ti64 rods in the rabbit femur demonstrated significantly higher bone apposition to the composite than Ti64 rods. The results of this study indicate that the invasion of surrounding bone cells and thus osteointegration together with its bone-matching mechanical properties make the PA12/CF/HA stem an interesting hip replacement candidate.

INTRODUCTION

Long-term fixation and rapid osseointegration of bone prostheses are the primary objectives in cementless joint replacement surgery. Furthermore, it is conceivable that for optimal osteointegration the properties of an ideal joint replacement, whether physical, mechanical or chemical, all have to match those of the host tissue. Since typical femoral components undergo millions of load cycles per year with loads averaging 4X body weight, the combination of alloys and implant designs capable of withstanding these demanding conditions for 15-20 year periods have historically resulted in relatively robust and stiff implants. Studies have repeatedly demonstrated a loss of proximal cortical bone stock attributed to the mismatch of stiffness between the high stiffness implant and the proximal femur. The phenomenon of bone loss adjacent to an implant is commonly referred to as "stress shielding" and generally occurs when a stiff implant is well fixed distally. It is believed that this encourages load transfer from the bearing couple through the implant to the bone in the region where distal fixation occurs. In this situation, load in the proximal femur is reduced and subsequent bone loss occurs, together with a concomitant increase in the risk of fixation failure. While progress at the bearing couple has reduced the particulate burden associated with osteolysis the same advances have not been made to reduce stress shielding. Based on the stiffness-related bone loss mechanism(s), it is conceivable that a femoral stem matching the cortical bone stiffness instead of simply possessing reduced stiffness as in previously cited works, would better reduce bone loss.

In the early 80's investigations with reduced-stiffness femoral components for the purpose of decreasing stress shielding observed with the relatively stiff commercially available CoCr femoral stems began [1-7]. These reduced-stiffness implants were subject to an increased incidence of loosening [1-3] as they failed to achieve proximal fixation. The design of these reduced stiffness femoral components had a common feature: they all had a bone fixation surface characterized by a low modulus of elasticity prone to high shear deformation. This low modulus fixation surface resulted in poor osseointegration and a predominantly fibrous interface [1,4,5]. Moreover, biomechanical studies showed that the expected advantageous bone loading and lower bone loss were not observed when stem fixation was obtained solely by press-fitting [6,7]. These observations prompted a series of studies on hybrid femoral stems with higher modulus and a porous coating. One example was a stem with a thin cobalt-chrome (Co-Cr) core, a intermediate layer of polyaryletherketone (PAEK) and fully porous titanium (Ti) mesh coating- Epoch (Zimmer, Warsaw, USA)[8-11]. The clinical experience with this stem confirmed the expected reduced bone loss, as well as stable initial and middle-term bone fixation. While these results demonstrate progress, the stiffness of this stem remains far from that of cortical bone to which it is fixed; based on equivalent bending stiffness calculations by Glassman [12] and Harvey [8], the equivalent modulus of elasticity of this porous Ti-coated PAEK overmolded Co-Cr stem is 54 GPa, approximately 250% above the typical modulus of elasticity of cortical bone of 15 GPa. As a result, stress shielding should also prevail to some extent on the mid to longer term with the latter femoral stems design.

Recent manufacturing advances [13-15] have enabled the development of fatigue

resistant, carbon fiber (CF) composite implants with stiffness characteristics matched to those of the human femur. A femoral stem has been fabricated that consists of three distinct material layers. The first is a long CF in a polyamide 12 (PA12) polymer matrix (PA12/CF), the second is a PA12/HA (hydroxyapatite) interface and the third a coating of hydroxyapatite (HA). A schematic representation of this composite stem is shown in Figure 1.

Figure 1: Schematic representation of the composite layers comprising the novel HA coated CF/PA12 femoral steam.

As previously reported, the HA-coated composite demonstrated very good chemical stability and mechanical adhesion of the plasma-sprayed HA coating [13]. Furthermore, the HA-coated composite showed a modulus of elasticity of 12.2 GPa, falling in the range of cortical bone modulus, as evaluated by Campbell *et al* [14]. Further biomechanical evaluations of the HA-coated composite femoral stem, validated through finite numerical analysis, indicated that it should enable better bone-implant interdigitation with reduced stress-shielding problems [15]. Therefore, the proposed implant with similar mechanical properties to that of cortical bone and an HA coating may hold promise as a means to reduce implant loosening associated with stress shielding.

The present paper presents *in vitro* and *in vivo* response to the HA-coated composite femoral stem. Although the interface to the biological environment will be the HA coating, the PA12/CF and PA12/HA layers were also individually tested *in vitro* as a precautionary measure in case of exposure to the bone environment. The proliferation of fibroblastic and osteoblast-like cells, as well as the specific phenotypic expression of osteoblast-like cells, were evaluated on the three different components of the prosthesis.

The L929 cell line is an established line of mouse fibroblasts recommended in cytotoxicity determinations due to their high sensitivity [17] and model properties that can serve to screen biomaterials [18]. The osteosarcoma-derived MG63 cell line is often used in *in vitro* models to explore the interactions between osteoblasts and biomaterials [19-21]. These two cell lines were chosen to assess cell-materials interactions in which fibroblasts are involved in healing the wound inflicted by stem insertion and osteoblasts derived from the adjacent marrow stem cells produce bone that attaches the stem to the surrounding trabecular lattice [22]. In addition to the cellular viability, three principal biochemical markers of osteoblast development were measured: alkaline phosphatase (ALP) expression, type I collagen (CICP) formation and osteocalcin (OC) expression. In addition, the response to an HA-coated CF/PA12 implant was evaluated in New Zealand White rabbits.

MATERIALS AND METHODS

Test materials preparation

The polymer composite for the THR stem consisted of a woven fabric of CF and PA12 fibers. Composite rods were obtained by moulding the composite fabric into 3.5 mm thick plates, from which round section rods were machined with a diameter of 3.2 mm. Prior to application of the HA coating, the surface of the composite rods was grit-blasted (24-grit, alumina oxide, resulting R_a of 6.38 μm), according to surface preparation of commercial hip stems (CLS stems, Zimmer, Warsaw, USA) and cleaned by a 2-step

ultrasonification procedure involving 99.9% ethanol and 98.9% acetone for 10 min cycles. The composite rods were then coated using atmospheric plasma spraying of HA particles using a proprietary technique to avoid thermal degradation of polymer composite substrate [23]. Commercially-available particles of fully crystalline HA (Captal 30, Plasma Biotal Ltd, Tideswell, UK) were used for plasma spraying. Granulometry testing on the initial HA powder (LS Particle Size Analyzer, Beckham Coulter, Fullerton, CA, USA) indicated a number-average diameter of 33 μm. Coatings of 80 μm in thickness were produced on all surfaces of the composite rods. The negative control used throughout the *in vitro* and *in vivo* study was medical grade extra low interstitial Ti-6Al-4V (Ti64) (Ti Industries, Montreal, Quebec, Canada). They were machined into 3.2 mm diameter rods. As the composite rods, the Ti64 rods were grit-blasted using the technique described above. The elastic modulus and density of the polymer composite and Ti64 used for the *in vitro* disks and *in vivo* rods are given in Table 1.

Table 1. Physico-mechanical properties of HA coated polymer composite and Ti-6Al-4V (negative control) used for the implant rods.

The surface roughness of the HA-sprayed composite was measured using a line profilometer (Surftest-211, Mitutoyo). Ten (10) measurements were made for each type of rod. Grit-blasted HA-coated composite and Ti64 rods showed non-statistically different roughness of 4.6 ± 0.5 μm and 4.5 ± 1.2 μm, respectively. Energy dispersive X-ray spectroscopic (EDS) analyses performed on the HA-coated surface of composite rods (6 measurements) led to an average Ca/P ratio of 1.69 ± 0.04, very close to the theoretical

HA Ca/P ratio of 1.67. X-ray diffraction (XRD) analyses on the HA-coated composite rods demonstrated that the crystalline index of the plasma-sprayed HA coating was 0.60 ± 0.04, predominantly (> 99%) composed of crystalline HA (Joint Committee on Powder Diffraction standard #9-432). EDS and XRD analyses on HA-coated composite rods indicate that the HA coating produced complied with ISO 13779-2 physicochemical requirements with respect to composition, crystalline index and Ca/P ratio.

In vitro water absorption and degradation studies

The *in vitro* water absorption and degradation studies of the polymer composites were performed by immersing samples in phosphate buffer solution (PBS) at a pH of 7.4. Pre-weighed, composite discs were immersed in 50-ml scintillation vials containing 24 ml of phosphate buffered saline (PBS). The vials were maintained in a shaker table (250 rpm) at 37°C and at predetermined times (1, 2, 3, 4, 8 and 12 weeks), the pH of the PBS solution was measured and the composite discs were removed from the PBS solution, surfaces thoroughly washed with distilled water to remove any adsorbed buffer salts, placed in a desiccators for 48 hrs and the weights recorded.

Ultrasonic cleaning and sterilization of samples

Samples were cleaned by a two-step ultrasonification procedure involving 99.9% ethanol and 98.9% acetone for 10 min cycles. The samples were then wrapped in plastic sterilization pouches and sterilized using pure ethylene oxide (EtO). EtO sterilization was carried out in SteriVac® (3M), with a 4-h cycle followed by 24 h sterile aeration to

remove residual EtO.

Cell cultures

Human derived osteoblast-like MG63 cells (ATCC, Rockville, MD, USA) and mouse fibroblasts L929 cell line (ATCC, Rockville, MD, USA) were used in this study. Cells were grown at 37°C in a 5% CO_2 humidified atmosphere in Eagle's Minimum Essential Medium (EMEM; ATCC, Rockville, MD, USA), supplemented with 10% heat-inactivated (56°C for 30 min) fetal bovine serum (FBS), 100 units/ml penicillin, and 100 μg/ml streptomycin (Gibco Laboratories, Burlington, ON, Canada).

Biocompatibility – Effect of material extracts

Preparation of the extracts

Extracts were prepared from the material samples in agreement with the ISO specification (10993-5) governing *in vitro* tests [24]. Each composite was immersed in EMEM at a ratio of 0.2 g/ml and incubated for 24 h at 37°C under constant agitation (250 rpm). After this period, the medium was harvested and kept at –90°C until used. The extracts were used undiluted and supplemented with 10%v/v FBS.

Cytotoxicity of composite extracts

The cytotoxicity of composite extracts was evaluated against L929 fibroblasts using the methyl tetrazolium (MTT) assay in 96-well plates as described by the manufacturer (Sigma-Aldrich). The MTT assay is based on the ability of living cells to convert a water-soluble yellow dye, 3-(4,5-dimethylthiazole-2-yl)-2,5-diphenyl tetrazolium bromide into

purple formazan crystals. Briefly, L929 cultured cells were seeded in 96-well plate (2.5×10^5 cells/ml, 200 µl/well) and allowed to adhere for 24 h at 37°C in a 5% CO_2 and 95% air humidified atmosphere. The culture medium was replaced by the previously prepared test medium, using normal EMEM medium as control, and further incubated for 24, 48 and 72 h. After the incubation periods, the extracts were removed and each well was treated with the MTT solution for 4 h at 37°C. Liquid was then removed, solubilization solution added, and microplate was shaken for 15 min before reading at 550 nm on a microplate reader. Control samples consisted of L929 cells grown on tissue culture plastic (TCP) supplemented with complete EMEM not in contact with fiber extracts. These methods have been reported previously for the evaluation of *in vitro* biocompatibility [25]. Cytotoxicity was calculated as the percentage of control cell viability. Results are the mean ± standard error of three (3) experiments performed in triplicate.

Direct contact cellular proliferation

Cell seeding

To test the long-term biocompatibility of the polymer composites, the sterilized samples were placed in 24-well plates. After the 5-day aeration time, the samples were soaked in PBS for 4 hours before cell seeding. A suspension of L929 or MG63 cells (1×10^4 cells/cm^2) was directly plated on each sample. The same number of L929 or MG63 cells was also plated on TCP and Ti64 as controls. Cells were allowed to attach for 2 h, then 900 µl of DMEM (Dulbecco Minimal Essential Medium) were added. Cultures were maintained in the conditions described above for 7 days, and the medium

was changed every 3 days.

Cell proliferation

The cell proliferation was monitored using the Alamar Blue™ assay according to the manufacturer (Biosource, Nivelles, Belgium). The assay is based on a fluorometric/colorometric growth indicator that detects metabolic activity. Specifically, the system incorporates an oxidation-reduction (REDOX) indicator that both fluoresces and changes colour in response to chemical reduction of growth medium resulting from cell growth [26]. The directly plated cells were incubated at 37°C in a humidified atmosphere of 5% CO_2 and 95% air. At selected time points of 1, 3 and 7 days, medium was removed and 1 ml aliquots of Alamar Blue (diluted 1:10 in phenol red-free medium) were added to each well and incubated for a further 4 hr at 37°C in 5% CO_2 and 95% air. Wells without cells were used as the blank control and cells grown on TCP and Ti64 supplemented with complete DMEM, were used as a negative control. Following the incubation 3 x 100 aliquots from each well were taken and transferred to a 96-well plate for reading. Absorbance was measured on an ELISA microplate reader at 570 nm. Numerical data were analyzed statistically using independent Student t tests. Statistical significance was considered at $p < 0.05$.

Cell morphology

MG63 osteoblast-like cell morphology, spreading, orientation, and growth on the surfaces of the composites were evaluated using the common qualitative technique, field emission gun scanning electron microscope (FEG-SEM) on a Hitachi S-4700 apparatus (Hitachi High-Technologies Canada Rexdale, Ontario). Harvested MG63 osteoblast-like cells were washed twice with PBS and fixed with 1% glutaraldehyde, first for 1 h at room

temperature, then overnight at 4°C. The samples were rinsed with PBS for 30 min and then dehydrated through a series of graded alcohol solutions. The specimens were air-dried overnight and the dry cellular constructs were finally sputter coated with palladium and observed under the FEG-SEM at an accelerating voltage of 2.0 kV.

MG63 bioactivity

ALP and OC content of the cell lysates as well as conditioned media and CICP of the conditioned media were evaluated only as determinants of osteoblast differentiation. ALP is a marker of differentiation and peaks as mineralization is initiated. OC, a late marker of differentiation, is associated with mineral deposition. CICP synthesis is a pre-requisite for the bone formation process and the later mineralization of collagen I fibers will lead to new bone accumulation around a stem. In order to examine the above osteoblast differentiation biochemical markers at 3, 7 and 14 days, the supernatants were collected and stored frozen at -20°C until assayed for ALP, OC and CICP. At each culturing period, the cellular cultures were lysed from the composite materials by gentle centrifugation and PBS washing, followed by 0.2% Triton X-100 cell lysis buffer addition. The lysed samples were preserved at -20°C until assaying for total protein determination, ALP and OC.

Protein determination

After 3, 7 and 14 days the protein concentration was measured in the cell lysates by the commercially available Micro BCA™ Protein Assay Reagent kit (Pierce Chemical Co, Rockford Illinois, USA). The assay was carried out according to the directions of the

manufacturer. Each sample was tested in triplicate using different dilutions and the optical density was measured by a microplate reader at 600 nm. The total protein content (μg/ml) was finally used for reference to normalize ALP activity, OC and CICP.

Alkaline Phosphatase Activity

The ALP activity, the driver of bone matrix mineralization, was determined in the cell lysates as well as the conditioned media at 3, 7 and 14 days. ALP was determined using a commercially available kit (AnaSpec, San Jose, CA) in accordance with the provided instructions. Briefly, the measurements were performed using 100 μl lysates or supernatants which 100 μl of *p*-nitrophenolphosphate dye was added. The enzyme ALP expressed by the cells hydrolyzes the substrate to p-nitrophenol and an inorganic phosphate. Under alkaline conditions, the p-nitrophenol was converted to a yellow product and its absorbance subsequently measured at 410 nm using a spectrophotometer. The absorbance was directly converted to ALP activity level based on a protein standard curve, which was obtained with bovine serum albumin (BSA). For each time point the activities in three samples were normalized as μmol per mg protein per min.

Osteocalcin assay

Osteocalcin levels were determined with a commercially available kit (ELISA, Biomedical Technologies, Inc., Stoughton, MA USA) in accordance with the provided instructions. The samples, as prepared above for the ALP assay, were added to the ELISA sample-buffer and homogenized via sonification. 100 μl of the samples (cell lysates or conditioned media) was placed into a 96-well plate, and incubated at 4°C for 24 h. After washing with PBS twice, 100 μl of an OC anti-serum was added to each well and 100 ml of donkey anti-goat IgG peroxidase was then added and incubated for 2 h at

room temperature. After washing with PBS twice, 100 µl of the substrate solution was added to the wells and incubated for 30 min at room temperature, which was then followed by adding 100 µl of an acidic stop solution. The absorbance was measured at 450 nm, and the OC expression level by the cells was determined based on an OC standard prepared in the range of 0.1–2 ng/ml and normalized as ng OC per mg of protein.

Collagen Assay

Collagen I synthesis was estimated indirectly from the concentration in the supernatants of the C-terminal propetide of type I collagen measured with the MertaCICP kit (Quidel corporations, CA, USA). The assay detects the extension peptides or propeptides cleaved from procollagen before incorporation of collagen into growing collagen fibrils. The release of these peptides into the supernatant accurately reflects collagen provides production by the MG63 cells plated on the different substrates. The test was performed according to the manufacturer's instructions.

Statistical Analysis

The *in vitro* cellular tests were performed on three (3) proliferation or four (4) differentiation replicate samples for each condition, and the data were represented as mean ± standard deviation (SD). Statistical difference was analysed using one-way analysis of variance (ANOVA), and p values < 0.05 were considered significant.

Osseointegration in a rabbit model

Animal model and implantation procedure

Nine New Zealand White rabbits (4.0 kg) were divided into two groups: one for the implantation of miniature composite THR stem and another for Ti64 miniature stem. The rabbits were housed in individual cages that were in the compliance with the guidelines of the Canadian Council on Animal Care. Implantation surgery was performed under a general inhalant anaesthetic (isoflurane) using standard aseptic techniques. Both back limbs were clipped and surgically prepped and each received one implant rod. For each limb a lateral, craniocaudal skin incision at the level of the patella was made. The subcutaneous layers were blunt dissected in order to expose the lateral joint capsule. The capsule was cut open for approximately 2 cm and the patella, quadriceps tendon and patella ligament were retracted medially to expose the epiphysis of the distal femur. The medullary canal was accessed via retrograde hand-drilling starting at the middle and distal extent of the femoral trochlea. The diameter of the intramedullary pin was approximately the same as the diameter of the implant rod. After insertion of the implant rod into the canal, the wound was rinsed with sterile saline. The joint capsule was closed with simple interrupted sutures using 4-0 absorbable sutures (polyglycolic acid). A simple continuous suture pattern, using the same suture material was also placed in both the subcutaneous space and subcutis. Anti-inflammatory, analgesic, and antibiotic medications were administrated post-surgically for 1, 3 and 5 days, respectively. The rabbit was allowed to bear full weight immediately after surgery.

Histomorphometry

After a post-implantation period (1 to 84 days), rabbits were euthanized under anaesthesia. The implanted femur specimens were isolated and cleaned. About 4 cm of the implanted end of the femur was cut off and fixed with 10% buffered formalin for 4

days with 4 changes. After gradual dehydration with ethanol from 70% to 95%, followed by 100% isopropanol and xylene, the specimens were infiltrated and embedded in methylmethacrylate/butyl methylmethacrylate according to Erben [26] and then allowed to polymerize. The implant-bone interface in the metaphyseal region was sectioned transversely and histologically examined. To do this, the tissue specimens were trimmed to the required position with a precision sectioning saw (Isomet 1000, Buehler) set at low-speed. A glass cover slip was then glued to the trimmed block surface to stabilize it. Approximately 200 μm thick sections were obtained after second cutting. These glass-attached sections were etched with 1% HCl in 70% ethanol for 1 h. After rinsing with water, the section specimens were stained with Sanderson's rapid bone staining (Fisher) for 40 min, followed by Acid fuchsin (0.134% Ponceau de xylidine, 0.034% Acid fuchsin, 0.2% glacial acetic acid in distilled water) for 40 min. The specimens were dipped in xylene and mounted on slides with Cytoseal mounting media (Richard Allan Scientific). Only the glass-free sides of the sections were stained and analyzed under bright-field microscope (Optiphot-2, Nikon).

Backscattered Scanning Electron Microscope (BSEM)

Undecalcified thin sections approximately 1 mm thick were made at 5mm intervals with a low-speed diamond blade saw (Buehler Corp, Markham, Ontario). High-resolution radiographs of the thin sections were obtained before additional analysis. The thin sections were prepared for backscattered scanning electron microscope (BSEM) imaging by progressively polishing the bone-implant surface down to 1200 silicon carbide paper, ultrasonically cleaning, drying and mounting on a stage, sputter coating with gold-palladium, and imaging in backscattered electron mode to produce a high resolution

image of the uppermost several microns of the bone-implant interface. Specimens were examined on a JEOL 840A Scanning Electron Microscope (JEOL, Peabody, MA) in compositional (backscatter) mode. Specimens were examined with an accelerating voltage of 15 kV at an average working distance of 39 mm and a probe current between 1×10^{-9} and 1×10^{-7} Amps. Using computer-aided image analysis, regions of bone in direct contact with the implant surface were measured, summed, and expressed as a percentage of the implant perimeter.

Statistical Analysis

The mean values and standard errors for bone apposition and period in days until rabbits recovered normal gait of (5) five implants and (4) four sections per implant groups were analyzed. The independent Student t test was used to determine the differences in bone apposition of the groups. Values of p less than 0.05 were considered statistically significant.

RESULTS

Composites weight loss and pH changes

The pH and weight change of the immersed HA-coated and non-coated PA12/CF components were measured following dynamic *in vitro* degradation experiments done in PBS at physiologic conditions. After 98 days, no weight had been lost. Indeed, the weights of both non-coated and coated composites had increased by 0.2% and 0.3% respectively, probably due to water absorption. After 1 week, half of the weight gain had

happened probably because of water absorption by both the hygroscopic PA12 matrix and the HA coating. No visible difference in morphology was noticed on the samples during and after the 98 days of immersion. The pH rose in the first week of immersion from pH of 7.4 to 7.6 and 7.8 for non-coated and coated composites, respectively, and then levelled off for the next 91 days. This increase was not significant ($p > 0.05$) for any of the samples.

Biocompatibility – Effect of material extracts

Cytotoxicity

The short-term effects of the composite degradation products on L929 fibroblasts viability are shown in Figure 1a. They clearly demonstrate that the products from all three composites did not significantly affect cell viability, which stayed around 100% from 24 to 72 h. As shown in Figure 2b, spindle-shaped cells with round-oval nuclei were seen on both the polystyrene TCP wells used as controls and on the composite-containing wells.

Figure 2a Effect of the composites extracts on the viability of L929 fibroblast cells as determined by the MTT assay. L929 cells were incubated in test medium (90 %v/v undiluted extracts - 10% v/v FBS) and the fibroblast viability was determined by the MTT assay at 24, 48 and 72 h. L929 cells grown on tissue culture plastic (TCP) supplemented with complete DMEM was used as the negative control. Results are expressed as % of negative control and are the mean ± standard deviation of 3 different experiments.

Figure 2b Representative optical microscope image of L929 cells incubated with HA composites extracts after 48 h (Only the cellular morphology following HA composite extracts is presented as it is representative of all other composites extracts).

Biocompatibility – Direct contact assay

Cell proliferation

As fibroblasts are cells present in virtually all tissues contributing to the proliferative phase of wound healing [22], their proliferation on the PA12/CF, PA12/HA and HA stem components was measured by the Alamar Blue assay, shown in Figure 3. The L929 fibroblast cultures grew equally well on the composites during the first 7 days. Moreover, there was no significant difference between the cultures on the three composites materials and those on Ti64 or TCP controls at any of the time points measured. Thus, the stem components were unlikely to interfere with initial implant wounding.

Osteoblast-like cells such as MG63 on the other hand are responsible for osteointegrating bone matrix synthesis (osteoid and prebone) and mineralization after the preliminary wound healing [22]. MG63 cell growth was also measured following seeding on the 4 materials at the same density as the L929 fibroblasts. During the first 3 days the MG63 cultures grew at the same rate on the 4 materials and as rapidly as the fibroblasts on the same materials (Fig. 3). However, between days 3 and 7 the osteoblasts started to proliferate faster than the fibroblasts (Fig. 3). Until day 7 there was no significant difference between MG63 cultures grown on the composite and control (Ti64 or TCP) materials. But by day 7 the MG63 cultures were growing significantly faster on the HA-

coated composites than on the Ti64 and TCP control materials and the PA12/CF, PA12/HA composite materials as well as faster than fibroblast cultures on all three composite materials.

Figure 3 Growth evaluation of MG63 and L929 cells seeded on CF/PA12, PA12/HA and HA composites. Cellular viability was assessed after 1, 3 and 7 days by the Alamar Blue assay. Negative control samples consisted of cells grown on tissue culture plastic (TCP) supplemented with complete DMEM. Results are the mean ± standard deviation of 3 different experiments.

MG63 bioactivity

Total Protein Content

The amount of protein in lysates of MG63 cultures on the HA-coated and other substrates is shown in Figure 4 as a function of incubation time. The total protein content, an indirect indicator of the number of cells in culture, indicated that at day 3, 7 and 14 there was no significant difference between the three different substrates evaluated (PA12/CF, PA12/HA and HA) and the Ti64 and TCP controls. The total protein content of the MG63 cells increased step-wise with the incubation time on the substrates and controls.

Figure 4 Total protein content of MG63 cells extracted from the composite materials over 2 weeks. Values are the mean ± SD of three cultures.

Osteocalcin

Osteocalcin (OC) is an important player in osteoblast-driven bone formation. It is primarily incorporated into the ECM of bone while only a small amount is released

directly into the circulation. The amounts of OC released into the medium were measured by assaying the supernatants of the MG63 cultures grown on the different composite materials for up to 14 days. As shown in Figure 5, values were normalized for the amount of protein per material and expressed in ng OC/mg total protein. By all three time points there were no significant differences between the OC levels released from the HA-coated composite and the other composite materials or controls. By day 7 the OC levels had peaked and by day 14 had returned to around day-3 values. The intracellular OC levels in the MG63 cells were also measured up to 14 days, but the values were too small to be accurately measured.

Alkaline Phosphatase activity

The activity of ALP, a membrane enzyme, is arguably the most commonly measured identifier of osteoblast activity. The ALP levels expressed by the cells were measured both in culture lysates (*i.e.*, intracellular ALP) and supernatants for up to 14 days. Values were normalized for the amount of protein per material and expressed in nmol/mg protein/min

Figure 5 Normalized Osteocalcin and ALP levels in medium of MG63 cells on the composite materials after 3, 7 and 14 days of culture. Values are the mean ± SD of three cultures.

As shown in Figure 5, by day 7 when the OC level had peaked, the amount of ALP released from the cells on the HA-coated PA12/CF composite was significantly higher than the levels from the MG63 cells on the other materials. By day 14 the ALP release

from the cells cultured on the HA-coated composite was even higher than the levels in the cultures on the other composite and control materials.

The amounts of ALP in lysates of the MG63 cells were at all times significantly less than the amounts released into the culture medium (Fig. 5). The average level of ALP in lysates was approximately 4 nMpi/mg of protein for all materials, including controls, with the exception of HA-coated composite at day 3 for which amounts of ALP in lysates were 8 nMpi/mg of protein. The latter was significantly more than the amounts of ALP in the lysates of the cells on the other composite materials and on the TCP and Ti64 controls. But by days 7 and 14, when the release into the medium raised the intracellular levels had fallen and there were no significant differences between the composite materials and controls.

Collagen I production

The amounts of type I collagen (CICP) released in the medium were measured by assaying the supernatants of the MG63 cultures on the different composite materials up to 14 days. As shown in Figure 6, values were normalized for the amount of protein per substrate material and expressed as ng CICP/mg total protein. While the levels tended to peak around day 7, the coating of the composite materials with HA did not significantly enhance CICP production.

Figure 6 Normalized CICP levels in medium of MG63 cells on the composite materials after 3, 7 and 14 days of culture.

Cell adhesion

The interactions between MG63 osteoblast-like cells and composites were studied *in vitro* by FEG-SEM for up to 14 days in culture (Fig. 7). Although all composites supported the attachment and spreading of MG63 osteoblasts, the filopodia extensions from the cells on the substrate were visually more abundant on HA-coated composites. As this study's main interest is the HA-covered composite, we focused on MG63 osteoblasts spreading on and penetrating into the PA12/HA composite. After the initial cell attachment on day 1, the HA surface was examined with SEM. Typical osteoblast morphology was seen as the planted cells were starting to spread and elongate. Up to day 7, the cells did not appear to closely contact the HA surface, which is a common artefact [13]. It should be noted that the HA surface was modified during its immersion in the culture medium, as precipitate appear to have formed on the surface of the HA coatings. Indeed after day 14 the osteoblasts appeared to be partly covered by precipitates from the culture medium as seen in Figure 7i. Similar precipitates were shown to correspond to apatite crystals re-deposited from the medium [13]. This covering might have helped the cells to integrate into the HA coating. Finally after day 14 the osteoblasts nearly covered the whole HA coating and with their filopodia extending into the crevices of the HA coating.

Figure 7 FEG-SEM images of: (a) typical surface morphology for HA plasma sprayed scaffolds at 100 μm scale and (b) at a 5 μm scale; and osteoblast morphology (c) after 1 day of MG63 plating at 200 μm scale, (d) after 1 day of MG63 plating zoomed to a 10 μm scale (e) after 7 day of MG63 plating at 100 μm scale, (f) after 7 day of MG63

plating zoomed to a 50 μm scale, (g) after 14 day of MG63 plating at 500 μm scale, (h) after 14 day of MG63 plating zoomed to a 50 μm scale; (i) MG63 surface partially covered with precipitates after 14 days of culture.

Osteointegration of femorally implanted composite rods

Animals were permitted unrestricted weight bearing and activity immediately after surgery. After a week, all rabbits had recovered and ambulation was normal. Results are summarized in Figure 8. These results indicate that although the average period until the rabbits recovered normal gait was shorter with Ti64 rods (3.6 ± 1.1 days) than with composite rods (5.5 ± 2.1 days), this difference was not statistically significant. After their sacrifice, the whole femurs were assessed for implant positioning by high resolution X-ray radiography (Fig. 9).

Figure 8 Period in days until rabbits implanted with Ti64 or composite rods recovered normal gait. Values are the mean ± SD of 5 rabbits for each type of rods; $p = 0.12 > 0.05$ for Ti64 vs composite rods.

Figure 9 X-ray *in situ* illustration of the position of a composite rod inserted into the femur of a male New Zealand White rabbit.

The bones were then sectioned, polished and stained for histological observations. Histological sections of the bones with implanted Ti64 or composite rods are shown in Figure 10. Observations of Ti64 rods revealed significant roughness from grit-blasting with particle debris remaining on the rods' surfaces. The surrounding trabecular bone adhered to, but did not penetrate the Ti64 implant surface (Fig. 10a). HA-coated composite rods also had surfaces roughened by grit-blasting, but there was no particle debris (Fig. 10b). However, there was a dramatic difference between the osteoblasts'

response to the HA-coated composite and the Ti64 rods. Osteoblasts and their progenitors from the surrounding trabeculae adhered to and then actually penetrated deeply into the HA coating giving a picture of strong osteointegration (Fig. 10b).

Figure 10 (a) Histological section of a femorally inserted Ti64 rod which shows the simple adherence without penetration of bone cells from adhering trabecular bone. (b) Histological section of composite rods showing bone apposition at HA coating plus bone penetration into the HA coating revealing substantial bridging and osteointegration.

Bone apposition was then quantified from SEM micrographs of these bone sections. Sections from single implanted bones are shown in Figure 11. SEM micrographs were then taken in backscattering electron mode for image analysis and bone apposition quantification. Ti64 rods were used as control for the implantation experiments. The sections of composite rod in Figure 11a show the apposition of the surrounding trabecular bone into the HA coating without the formation of fibrous layer encapsulation; whereas the sections of Ti64 rods in Figure 11b show bone apposition and fibrous layer encapsulation. The levels of bone apposition to both Ti64 and composite rods are reported in Figure 12. This figure indicates that bone apposition to the Ti64 rods was significantly lower ($22.4 \pm 14.2\%$) than to the composite rods ($34.1 \pm 15.0\%$) if statistical significance is taken at $p = 0.04 < 0.05$ for 5 analysed implants and 4 sections per implant.

Figure 11 a) (left-side) Micrograph of composite-implanted bone section and (right-side) backscattering electron SEM micrographs showing apposition and penetration of the surrounding trabecular bone into a HA covered composite rod without an intervening fibrous layer encapsulation. Fibrous structure of

composite with fiber bundles is clearly visible. Large voids also appear in the centre of the rods as a result of damage produced by sectioning and imperfect composite consolidation. b) (left-side) Micrograph of Ti64-implanted bone section and (right-side) backscattering electron SEM micrograph showing bone apposition (light gray) on Ti64 rod (bright gray) and fibrous layer encapsulation. Large voids also appear in the centre of the rods as a result of damage produced by sectioning.

Figure 12 Bone apposition at the surface of the composite and Ti64 rods reported as the fraction in percent of measured rod perimeter covered with bone. Bone apposition was obtained from four sections of each of five implants of each type of rod. Values are the mean ± SD; $p = 0.008 < 0.05$ for Ti64 vs composite rods.

DISCUSSION

Recently, significant attention has been given to the composite approach in material development for hard tissue replacements with a particular emphasis on mechanical and biological similarities to the tissues being replaced. The trend of combining two or more materials to produce a composite drawing on the advantages of each to make a superior material has become a sound alternative. In the goal of reducing bone loss resulting from stress shielding and associated long-term fixation problems, this paper proposes the use of a custom-made composite for femoral stem with bone-matching stiffness [15,27]. Consequently the interest in the novel cortical bone-like PA12/CF composite as a potential THR stem comes from its mechanical properties similar to that of cortical bone demonstrated in our previous studies [14,15]. The purpose of this study was to evaluate the *in vitro* and *in vivo* biological properties of the novel composites for eventual THR applications. Although the true interest of the *in vitro* biological interactions was the HA-coated part of the prosthesis because, it will be in direct contact with the femoral bone, its

sub-components, *i.e.,* PA12/CF composite and PA12/HA interface material, were also evaluated as a precautionary measure in case of accidental exposure to surrounding bone cells. The control used throughout the *in vitro* and *in vivo* study was grit-blasted Ti64, because it is commonly used orthopaedic biomaterial associated [28].

The *in vitro* behavior of MG63 osteoblast-like cells on biomaterials is characterized by the normal sequence of cell adhesion, proliferation, differentiation, matrix synthesis and finally matrix mineralization [29]. Cell adhesion and spreading are the first steps of cell-material interactions. Therefore SEM analyses were carried out on MG63 cell planted on the three materials: HA, PA12/CF and PA12/HA. The SEM observations showed that all composites supported osteoblastic attachment and spreading, but filopodia extensions from the cells on and into the substrate were visually more abundant on HA-coated composites. Such greater filopodial probing determines the cells responses, be it only adherence to or proliferation on and penetration into their substrate [30]. In other words, the strength and extent of the initial cellular attachment and the signals it generates will influence the cells further proliferation and differentiation [30]. Thus, after 7 days in culture, the osteoblastic viability, determined by the direct contact (Alamar Blue) assay, was significantly higher on the HA-coated composite than on the PA12/CF and PA/HA composites. Furthermore the osteoblastic MG63s' viability on the PA12/CF and PA/HA composites (component materials of the stem) was at least equal to the viability on the Ti64 and TCP negative controls, which means acceptable osteoblastic biocompatibility. On the other hand L929 fibroblastic viability was the same on all substrates which also

indicates acceptable biocompatibility of all three composites for the initial implant wound-healing fibroblasts.

As previously mentioned, in the normal sequence of cellular events, cellular adhesion and proliferation are followed by the differentiation of proliferating immature osteoprogenitor cells into proliferatively shut-down mature osteoblasts which make surface-bonding bone matrix and penetrate into the implant surface. Thus, more important for a candidate THR material is its ability to support osteogenic differentiation and with it osteointegration. Therefore we compared the *in vitro* abilities of the various materials to differentiation of osteoblastic MG63 cells as indicated by their expression of the most important ALP, as well as OC and CICP.

A striking surging of ALP activity into the medium of MG63 cultures on HA-coated composites which had started by day 7 and had risen to much higher levels by 14 days than in the media of cultures on uncoated composites as well as Ti64 and TCP controls. This significantly higher ALP release from HA-coated composites meant higher osteoblastic differentiation potential as ALP is known for its apatite crystals deposition in the differentiation phase [31]. Additionally after a week of co-culture the osteoblasts appeared to be partly covered by crystals deposition as it was visually observed (Figure 7i).

OC synthesis was quantified next, as OC a calcium-binding polypeptide plays a fundamental role in bone remodelling and represents the specific marker in late stage

osteoblastic differentiation. Although MG63 cells grown on PA12/CF, HA-coated PA12/CF and PA12/HA released about the same amounts of OC, these levels were nevertheless higher than in cultures grown on the negative control materials. The OC levels from the MG63 cells on the HA-coated composite were at least twice as high as the reported levels from normal and osteopenic bone-derived osteoblasts [32] and MG63 osteoblasts [33] cultured on other novel prosthetic materials. On balance this would indicate the enhanced driving of OC production and function of osteoblasts on our novel composite surfaces.

The HA coatings did not promote production of collagen I as indicated by CICP levels. Literature on the influence of implant materials on CICP production is contradictory. Scotchford [28] has reported the ability of novel carbon fiber composites to increase CICP by cells growing on it while Montanaro *et al.* [33] have found that a nickel-free stainless steel does not.

Overall our results indicate that the PA12/CF, HA-coated PA12/CF and PA12/HA materials are cytocompatible materials, on which immature osteoblastic cells can adhere, spread, proliferate and regularly differentiate. Indeed the HA coatings promoted the expression of some key osteoblastic markers with respect to TCP and Ti64.

The suggestion of a promotion of osteogenic differentiation by HA coating by the results of our *in vitro* experiments prompted us to study the composite material behavior in New Zealand White rabbits. This well-known rabbit model was used to demonstrate the

striking osteointegration of a miniature femoral stem composed of all three above analyzed components, *i.e.*, HA-coated CF/PA12 rods, in comparison to the response to a similar stem made of Ti64 with an equivalent surface roughness (R_a). Bone apposition obtained at 7 weeks for both the composite rods (34.1 ± 15.0%) and the Ti64 rods (22.4 ± 14.2%) compares very well with results reported in New Zealand white rabbits, from intramedullary Ti64 femoral rods (5 mm) that showed bone apposition of the order of 10-16% after 6 weeks (Stewart et al. [34]), 24% after 6 weeks (Stangl et al. [35]) and 12% after 6 weeks (Tisdel et al. [36]). Of particular interest is a study by Feighan et al. [37] who compared polished ($R_a < 0.1$ μm) to grit-blasted ($R_a \approx$ 5-7 μm) intramedullary 5 mm Ti64 rods in New Zealand white rabbits and reported bone apposition of respectively 10% for the polished and 28% for the grit-blasted rods after 6 weeks.

CONCLUSIONS

The results of these experiments support the continued development of novel PA12/CF composite bone implants with an HA coating. *In vivo* the osteoprogenitor cells from the adjacent femoral trabecular bone adhere to and penetrate into the HA-coated composite implants. *In vitro* all three different implant components support osteoblast-like cells proliferation, and HA-coated components induced superior bioactivity as seen by increases in ALP and OC expression. Although, these results clearly indicate interest in the HA-coated composite stem with bone-matching stiffness as a new durable product for hip arthroplasty long term animal trials of actual hips should still be performed.

ACKNOWLEDGEMENTS

We thank Dr Craig Bihun for implanting the stems in the rabbit femurs and Drs. A. Candeliere and Shen Hui for their advice in designing the rabbit experiments. We also thank Alain Drouin and Virginia Ross for preparing the femoral sections and the histomorphological analyses of the sections.

REFERENCES

1. Tullos HS, McCaskill BL, Dickey R, Davidson J. Total hip arthroplasty with a low-modulus porous-coated femoral component. J Bone Joint Surg Am. 1984;66(6):888-898.

2. Jacobsson SA, Djerf K, Gillquist J, Hammerby S, Ivarsson I. A prospective comparison of Butel and PCA hip arthroplasty. J Bone Joint Surg Br.1993;75-B(4):624-629.

3. Niinimaki T, Puranen J, Jalovaara P. Total hip arthroplasty using isoelastic femoral stems. A seven- to nine-year follow-up in 108 patients. J Bone Joint Surg Br. 1994;76-B(3):413-418.

4. Spector M. Noncemented hip implants. Factors augmenting or inhibiting biological fixation. Hip. 1987:213-224.

5. Poss R, Walker P, Spector M, Reilly DT, Robertson DD, Sledge CB. Strategies for improving fixation of femoral components in total hip arthroplasty. Clin Orthop Relat Res. 1988(235):181-194.

6. Vail TP, Glisson RR, Koukoubis TD, Guilak F. The effect of hip stem material modulus on surface strain in human femora - Design vs materials vs interface J Biomechanics. 1998;31(7):619-628.

7. Simões JA, Vaz MA. The influence on strain shielding of material stiffness of press-fit femoral components. Proc Inst Mech Eng. 2002;216(5):341-346.

8. Harvey EJ, Bobyn JD, Tanzer M, Stackpool GJ, Krygier JJ. Effect of Flexibility of the Femoral Stem on Bone-Remodeling and Fixation of the Stem in a Canine Total Hip Arthroplasty Model without Cement. J Bone Joint Surg Am. 1999;81(1):93-107.

9. Kärrholm J, Anderber C, Snorrason F, Thanner J, Langeland N, Malchau H, et al. Evaluation of a Femoral Stem with Reduced Stiffness : A Randomized Study with Use of Radiostereometry and Bone Densitometry. J Bone Joint Surg Am. 2002;84(9):1651-1658.

10. Akhavan S, Matthiesen MM, Schulte L, Penoyar T, Kraay MJ, Rimnac CM, et al. Clinical and Histologic Results Related to a Low-Modulus Composite Total Hip Replacement Stem. J Bone Joint Surg Am. 2006;88(6):1308-1314.

11. McAuley JP, Engh CAJr. Femoral fixation in the face of considerable bone loss: cylindrical and extensively coated femoral components. Clin Orthop Relat Res. 2004(429):215-221.

12. Glassman AH, Crowninshield RD, Schenck R, Herberts P. A Low Stiffness Composite Biologically Fixed Prosthesis. Clinical Orthopaedics & Related Research. 2001(393):128-136.

13. Auclair-Daigle C, Bureau MN, Legoux J-G, Yahia L'H. Bioactive hydroxyapatite coatings on polymer composites for orthopedic implants J Biomed Mater Res Pt A.73A(4):398-408.

14. Campbell M, Bureau NM, Yahia L. Performance of CF/PA12 composite femoral stems. J Mater Sci: Mater Med. 2007; DOI 10.1007/s10856-007-3073-y.

15. Bougherara H, Bureau MN, Campbell M, Vadean A, Yahia L'H. Design of a biomimetic polymer-composite hip prosthesis. J Biomed Mater Res A 2007;82(A):24-40

16. Soballe K. Hydroxyapatite ceramic coating for bone implant fixation: Mechanical and histological studies in dogs. Acta Orthop Scand. 1993; 64 (255) 1-58

17. Neumann A, Reske T, Held M, Jahnke K, Ragoay C, Maier HR. Comparative investigation of the biocompatibility of various silicon nitride ceramic qualities in vitro. J Mater Sci: Mater Med. 2004;15(10):1135-1140.

18. Timmer MD, Shin H, Horch RA, Ambrose CG, Mikos AG. In Vitro Cytotoxicity of Injectable and Biodegradable Poly(propylene fumarate)-Based Networks: Unreacted Macromers, Cross-Linked Networks, and Degradation Products. Biomacromolecules. 2003;4(4):1026-1033.

19. Kirkpatrick CJ, Mittermayer C. Theoretical and practical aspects of testing potential biomaterialsin vitro. J Mater Sci Mater Med. 1990;1(1):9-13.

20. Clover J, Gowen M. Are MG-63 and HOS TE85 human osteosarcoma cell lines representative models of the osteoblastic phenotype. 1994;15(6):585-591.

21. Campoccia D, Arciola CR, Cervellati M, Maltarello MC, Montanaro L. In vitro behaviour of bone marrow-derived mesenchymal cells cultured on fluorohydroxyapatite-coated substrata with different roughness. Biomaterials. 2003;24(4):587-96.

22. Ziats NP, Miller KM, Anderson JM. In vitro and in vivo interactions of cells with biomaterials. Biomaterials. 1988;9(1):5-13.

23. Bureau NM, Legoux JG, Bélanger S. Tie layer for thermal spray coatings on thermoplastic-based materials'' S. US Provisional Patent Application, no 60/643,599

24. ANSI/AAMI/ISO, 10993-5. Biological evaluation of medical devices, Part 5: Tests for in vitro cytotoxicity. 1999.

25. Marques AP, Reis RL, Hunt JA. The biocompatibility of novel starch-based polymers and composites: in vitro studies. Biomaterials. 2002;23(6):1471-8.

26. Ahmed SA, Gogal Jr , Walsh JE . A new Rapid and Simple Non-Radioactive assay to Monitor and Determine the proliferation of Lymphocytes: An Alternative to H3-thymidine incorporation assay. . J Immunol Meth. 1994(170):211-24.

27. Kalpana SK. Biomaterials in total joint replacement. Colloids Surf, B. 2004;39(3):133-42.

28. Scotchford CA, Garle MJ, Batchelor J, Bradley J, Grant DM. Use of a novel carbon fibre composite material for the femoral stem component of a THR system: in vitro biological assessment. Biomaterials. 2003;24(26):4871-9.

29. Xue W, Moore JL, Howard LH, Susmita B, Amit B, et al. Osteoprecursor cell response to strontium-containing hydroxyapatite ceramics. J Biomed Mater Res, A. 2006;79A(4):804-14.

30. Gyu Ha R, Won-Sun Y, Hye-Won R, In-Seop L, Gun Hwan L, et al. Plasma surface modification of poly (d,l-lactic-co-glycolic acid) (65/35) film for tissue engineering. Surf Coat Technol. 2005;193(1-3):60-4.

31. Stucki U, Schmid J, Hammerle CF, Lang NP. Temporal and local appearance of alkaline phosphatase activity in early stages of guided bone regeneration.A descriptive histochemical study in humans. Clin Oral Implant Res 2001;12:121-7.

32. Torricelli P, Verné E, Brovarone CV, Appendino P, Rustichelli F, Krajewski A, et al. Biological glass coating on ceramic materials: in vitro evaluation using primary osteoblast cultures from healthy and osteopenic rat bone. Biomaterials. 2001;22(18):2535-43.

33. Montanaro L, Cervellati M, Campoccia D, Arciola CR. Promising in vitro performances of a new nickel-free stainless steel J Mater Sci: Mater Med. 2006:267-75.

34. Stewart M, Welter JF, Goldberg VM. Effect of hydroxyapatite/tricalcium-phosphate coating on osseointegration of plasma-sprayed titanium alloy implants. J Biomed Mater Res A. 2004;69A(1):1-10.

35. Stangl R, Pries A, Loos B , Müller M, Erben RG . Influence of pores created by laser superfinishing on osseointegration of titanium alloy implants. J Biomed Mater Res A. 2004;69A:444-53.

36. Tisdel CL, Goldberg VM, Parr JA, Bensusan JS, Staikoff LS, Stevenson S. The influence of a hydroxyapatite and tricalcium-phosphate coating on bone growth into titanium fiber-metal implants. J Bone Joint Surg Am. 1994;76(2):159-71.

37. Feighan JE, Goldberg VM, Davy D, Parr JA, Stevenson S. The influence of surface-blasting on the incorporation of titanium-alloy implants in a rabbit intramedullary model. J Bone Joint Surg Am. 1995;77(9):1380-95.

* Title Page

Novel carbon fiber composite with bone matching stiffness for hip replacement with improved *in vitro* and *in vivo* osseointegration

S. Dimitrievska[1], J. Whitfield[2], SA. Hacking[3], M. N. Bureau[1]

[1] Industrial Materials Institute – National Research Council Canada

75 de Mortagne blvrd, Boucherville, QC J4B 6Y4, Canada

[2] Institute for Biological Sciences – National Research Council Canada

[3] Division of Orthopaedics, McGill University, Montreal QC Canada

Captions

Figure 1: Schematic representation of the composite layers comprising the novel HA coated CF/PA12 femoral steam.

Figure 2a Effect of the composites extracts on the viability of L929 fibroblast cells as determined by the MTT assay. L929 cells were incubated in test medium (90 %v/v undiluted extracts - 10% v/v FBS) and the fibroblast viability was determined by the MTT assay at 24, 48 and 72 h. L929 cells grown on tissue culture plastic (TCP) supplemented with complete DMEM was used as the negative control. Results are expressed as % of negative control and are the mean ± standard deviation of 3 different experiments.

Figure 2b Representative optical microscope image of L929 cells incubated with HA composites extracts after 48 h (Only the cellular morphology following HA composite extracts is presented as it is representative of all other composites extracts).

Figure 3 Growth evaluation of MG63 and L929 cells seeded on CF/PA12, PA12/HA and HA composites. Cellular viability was assessed after 1, 3 and 7 days by the Alamar Blue assay. Negative control samples consisted of cells grown on tissue culture plastic (TCP) supplemented with complete DMEM. Results are the mean ± standard deviation of 3 different experiments.

Figure 4 Total protein content of MG63 cells extracted from the composite materials over 2 weeks. Values are the mean ± SD of three cultures.

Figure 5 Normalized Osteocalcin and ALP levels in medium of MG63 cells on the composite materials after 3, 7 and 14 days of culture. Values are the mean ± SD of three cultures.

Figure 6 Normalized CICP levels in medium of MG63 cells on the composite materials after 3, 7 and 14 days of culture.

Figure 7 FEG-SEM images of: (a) typical surface morphology for HA plasma sprayed scaffolds at 100 μm scale and (b) at a 5 μm scale; and osteoblast morphology (c) after 1 day of MG63 plating at 200 μm scale, (d) after 1 day of MG63 plating zoomed to a 10 μm scale (e) after 7 day of MG63 plating at 100 μm scale, (f) after 7 day of MG63 plating zoomed to a 50 μm scale, (g) after 14 day of MG63 plating at 500 μm scale, (h) after 14 day of MG63 plating zoomed to a 50 μm scale; (i) MG63 surface partially covered with precipitates after 14 days of culture.

Figure 8 Period in days until rabbits implanted with Ti64 or composite rods recovered normal gait. Values are the mean ± SD of 5 rabbits for each type of rods; $p = 0.12 > 0.05$ for Ti64 vs composite rods.

Figure 9 X-ray *in situ* illustration of the position of a composite rod inserted into the femur of a male New Zealand White rabbit.

Figure 10 (a) Histological section of a femorally inserted Ti64 rod which shows the simple adherence without penetration of bone cells from adhering trabecular bone. (b) Histological section of composite rods showing bone apposition at HA coating plus bone penetration into the HA coating revealing substantial bridging and osteointegration.

Figure 11 a) (left-side) Micrograph of composite-implanted bone section and (right-side) backscattering electron SEM micrographs showing apposition and penetration of the surrounding trabecular bone into a HA covered composite rod without an intervening fibrous layer encapsulation. Fibrous structure of composite with fiber bundles is clearly visible. Large voids also appear in the centre of the rods as a result of damage produced by sectioning and imperfect composite consolidation. b) (left-side) Micrograph of Ti64-implanted bone section and (right-side) backscattering electron SEM micrograph showing bone apposition (light gray) on Ti64 rod (bright gray) and fibrous layer encapsulation. Large voids also appear in the centre of the rods as a result of damage produced by sectioning.

Figure 12 Bone apposition at the surface of the composite and Ti64 rods reported as the fraction in percent of measured rod perimeter covered with bone. Bone apposition was obtained from four sections of each of five implants of each type of rod. Values are the mean ± SD; $p = 0.008 < 0.05$ for Ti64 vs composite rods.

Table 1. Physico-mechanical properties of HA coated polymer composite and Ti-6Al-4V (negative control) used for the implant rods.

Figure 1

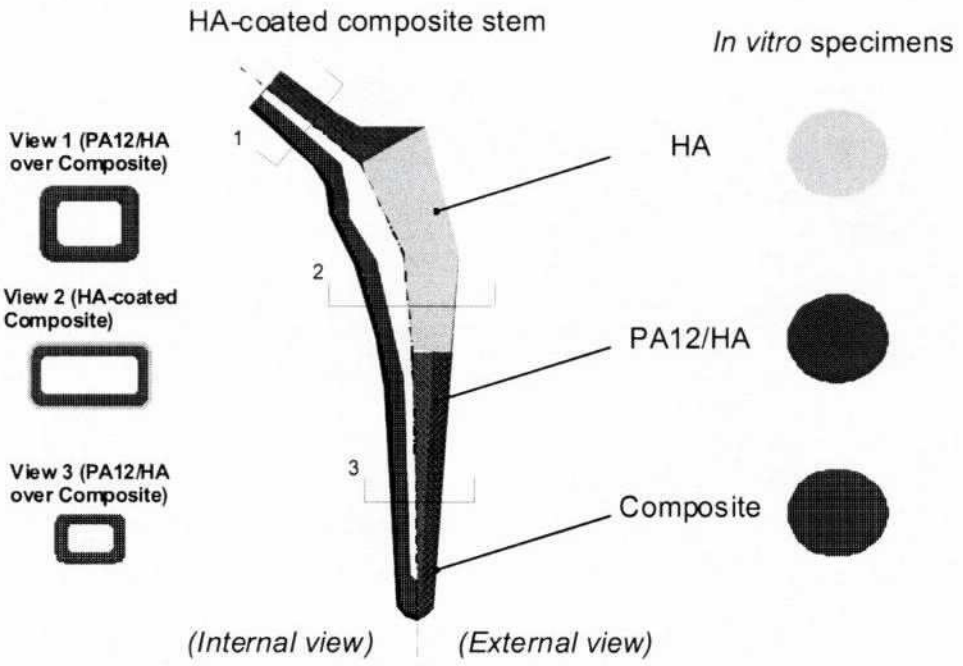
HA-coated composite stem
In vitro specimens
View 1 (PA12/HA over Composite)
View 2 (HA-coated Composite)
View 3 (PA12/HA over Composite)
1
2
3
HA
PA12/HA
Composite
(Internal view)
(External view)

Figure 2

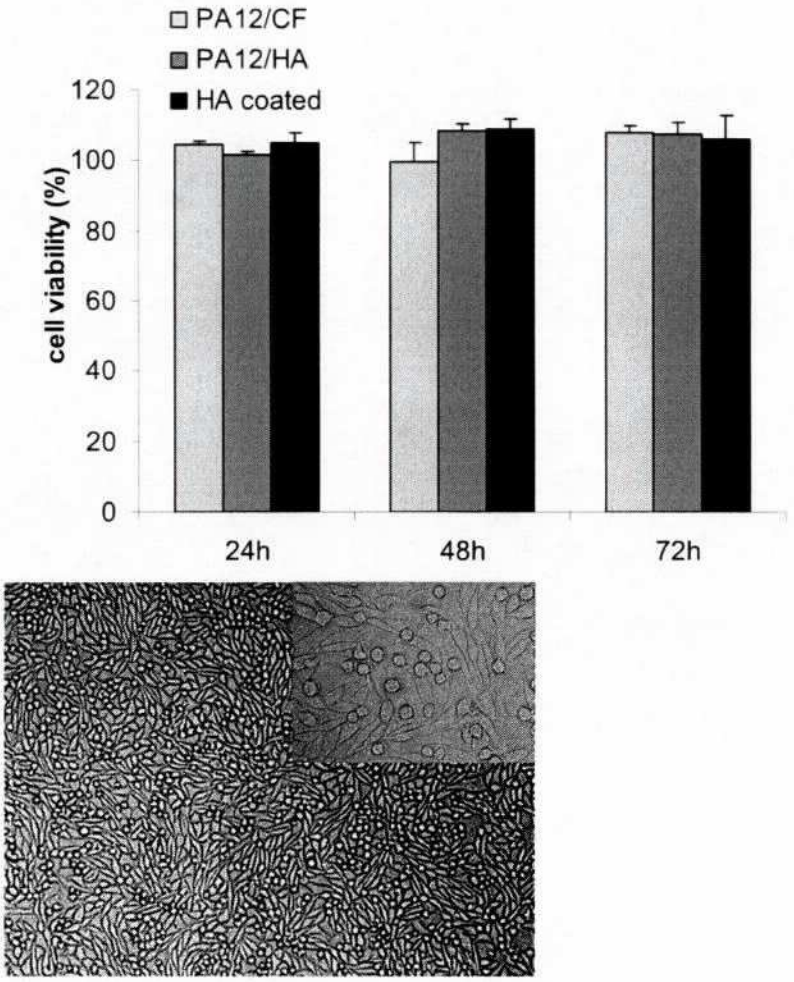
PA12/CF
PA12/HA
HA coated
cell viability (%)
120
100
80
60
40
20
0
24h
48h
72h

Figure 3

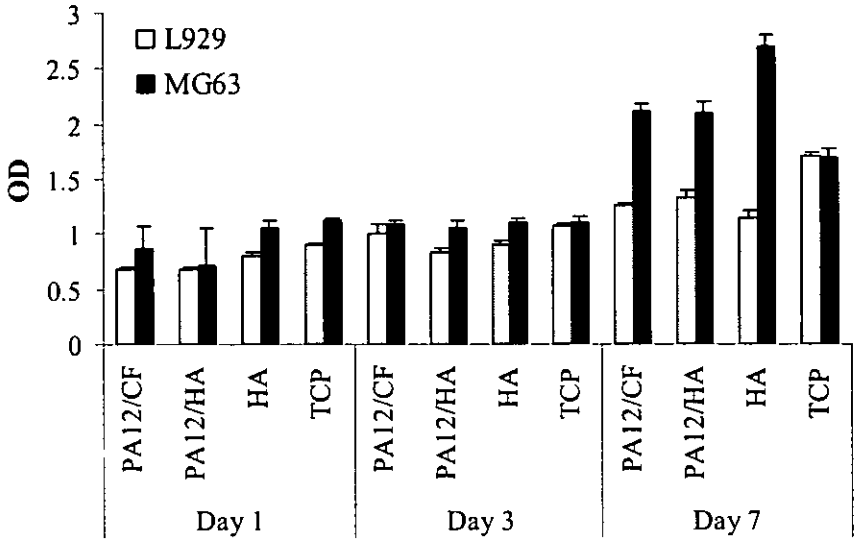
L929
MG63
OD
3
2.5
2
1.5
1
0.5
0
PA12/CF
PA12/HA
HA
TCP
PA12/CF
PA12/HA
HA
TCP
PA12/CF
PA12/HA
HA
TCP
Day 1
Day 3
Day 7

Figure 4

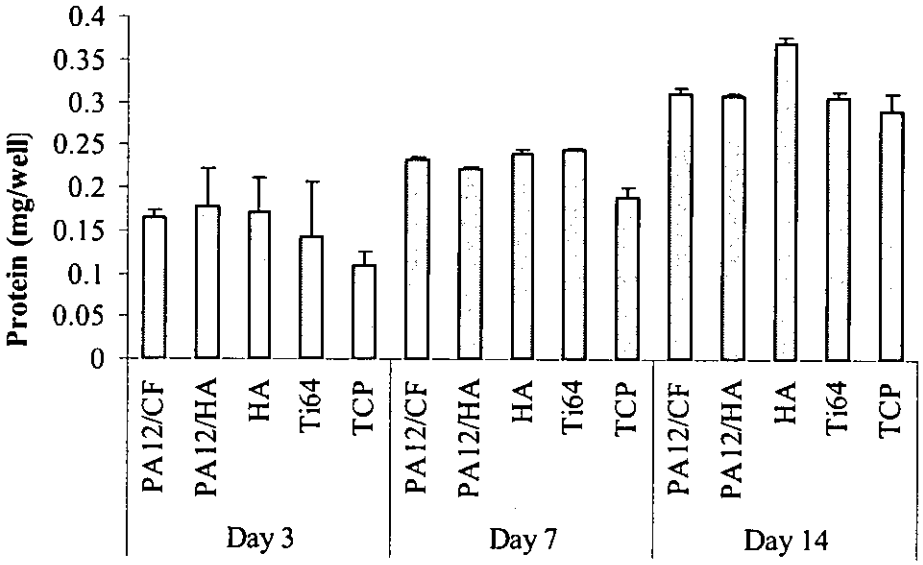
Protein (mg/well)
0.4
0.35
0.3
0.25
0.2
0.15
0.1
0.05
0
PA12/CF
PA12/HA
HA
Ti64
TCP
Day 3
Day 7
Day 14

Figure 5

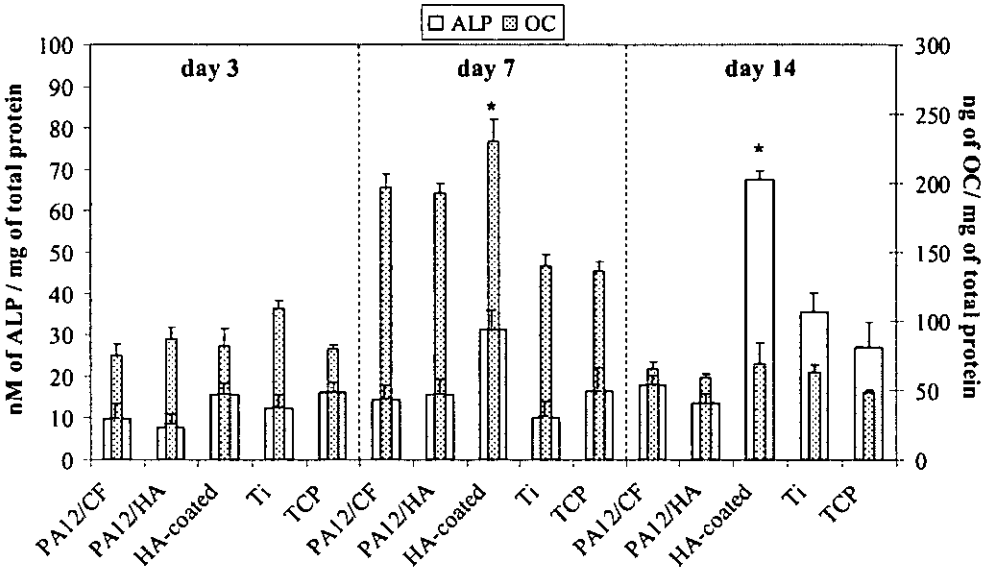
ALP
OC
day 3
day 7
day 14
nM of ALP / mg of total protein
ng of OC/ mg of total protein
0
10
20
30
40
50
60
70
80
90
100
0
50
100
150
200
250
300
*
*
PA12/CF
PA12/HA
HA-coated
Ti
TCP
PA12/CF
PA12/HA
HA-coated
Ti
TCP
PA12/CF
PA12/HA
HA-coated
Ti
TCP

Figure 6

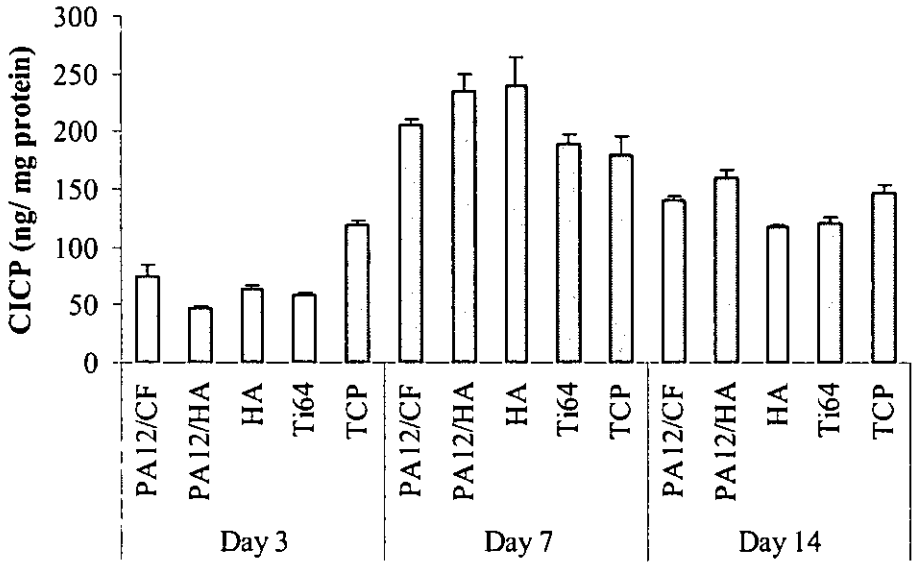
CICP (ng/ mg protein)
300
250
200
150
100
50
0
PA12/CF
PA12/HA
HA
Ti64
TCP
Day 3
Day 7
Day 14

Figure 7

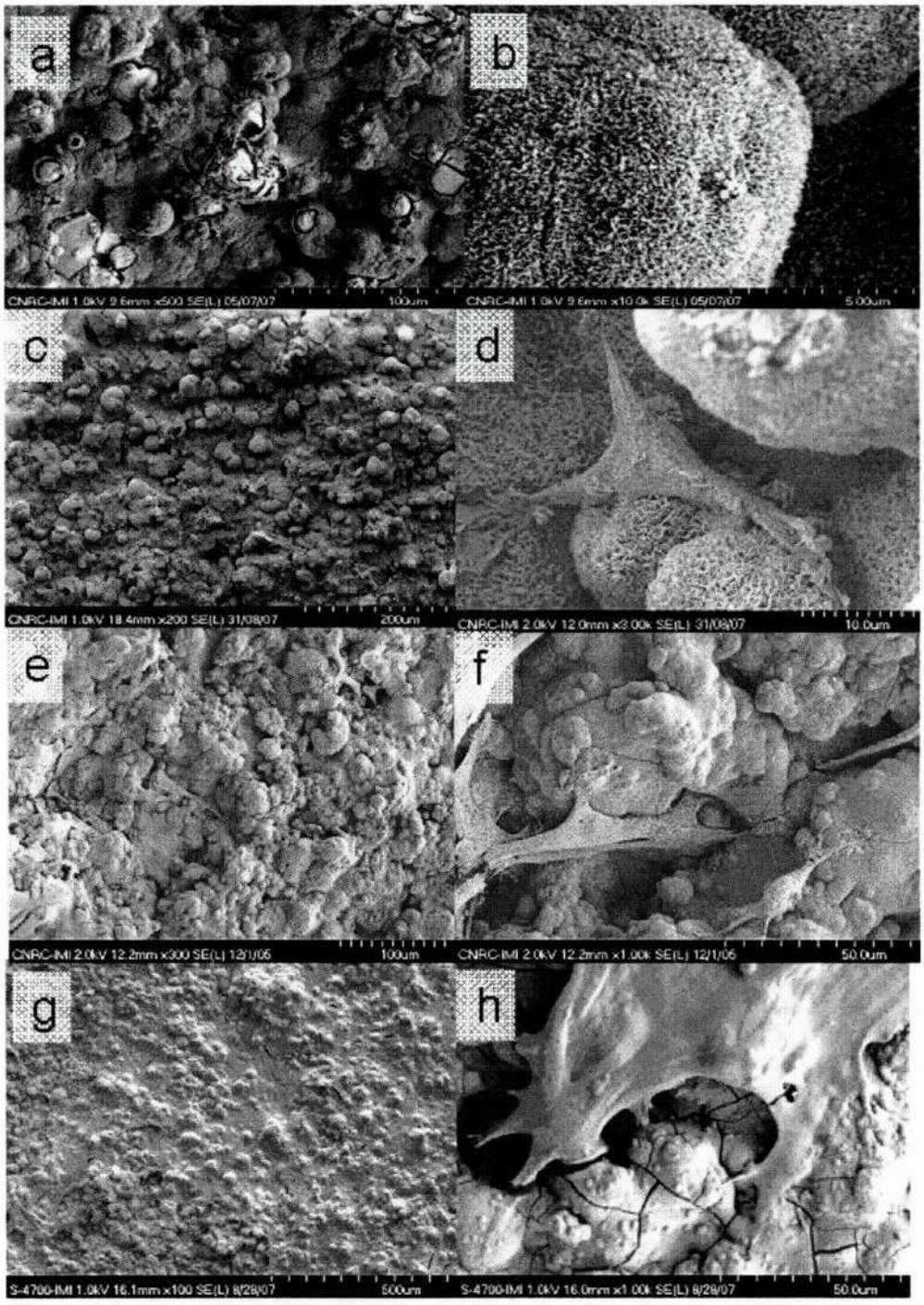
a
b
c
d
e
f
g
h
CNRC-IMI 1.0kV 9.6mm x500 SE(L) 05/07/07 100um
CNRC-IMI 1.0kV 9.6mm x10.0k SE(L) 05/07/07 5.00um
CNRC-IMI 1.0kV 18.4mm x200 SE(L) 31/08/07 200um
CNRC-IMI 2.0kV 12.0mm x3.00k SE(L) 31/08/07 10.0um
CNRC-IMI 2.0kV 12.2mm x300 SE(L) 12/1/06 100um
CNRC-IMI 2.0kV 12.2mm x1.00k SE(L) 12/1/06 50.0um
S-4700-IMI 1.0kV 16.1mm x100 SE(L) 8/28/07 500um
S-4700-IMI 1.0kV 16.0mm x1.00k SE(L) 8/28/07 50.0um

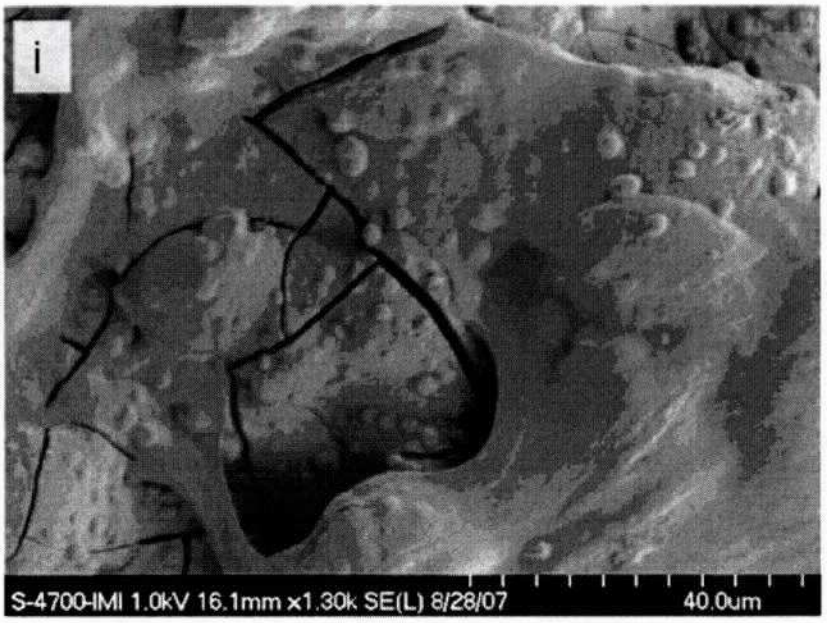
i
S-4700-IMI 1.0kV 16.1mm x1.30k SE(L) 8/28/07
40.0um

Figure 8

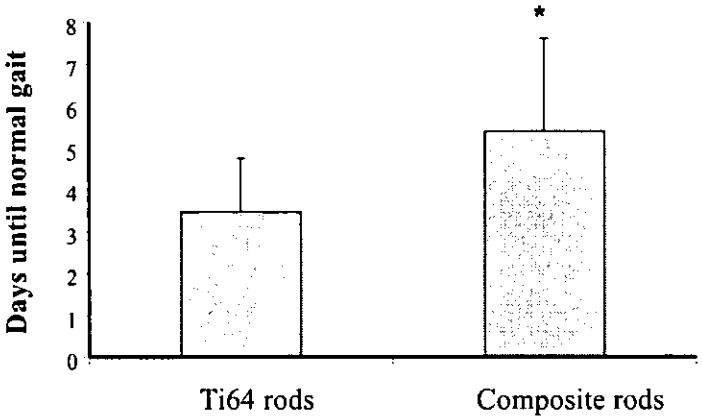

Figure 9

Figure 10

a)

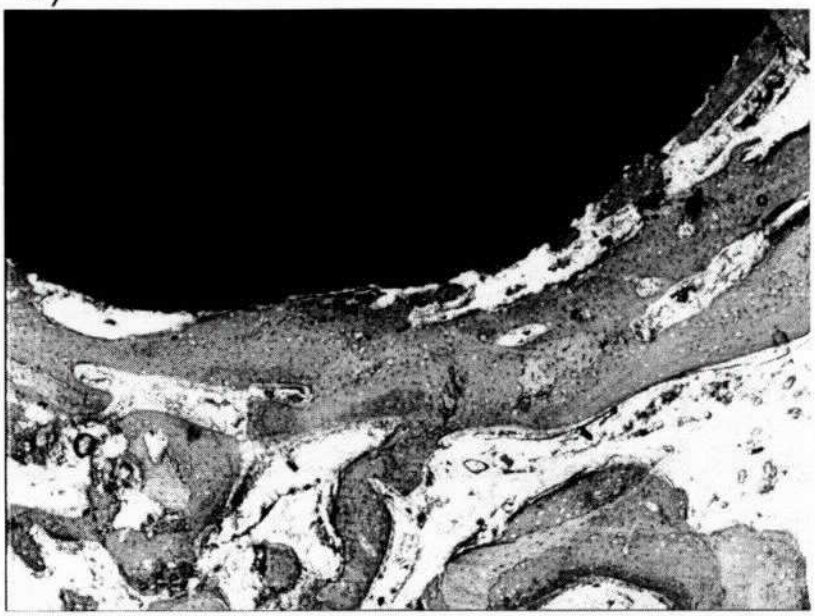

b)

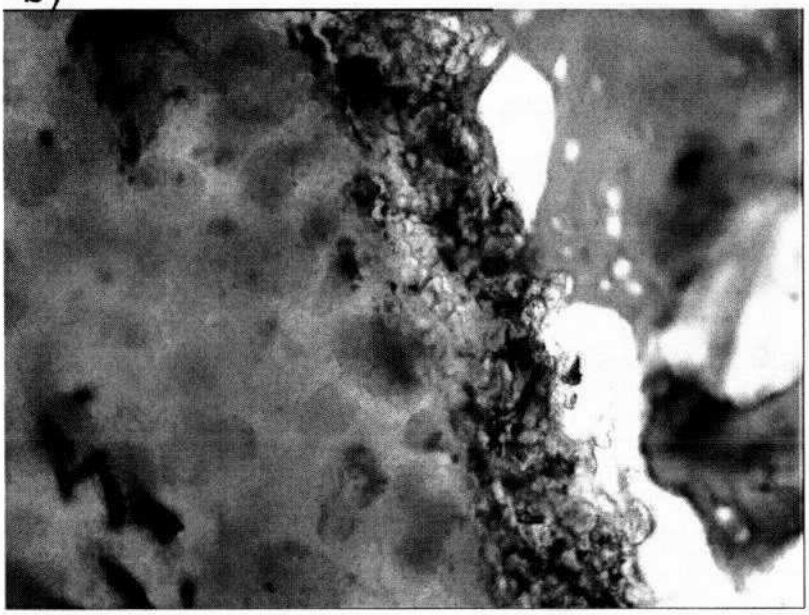

Figure 11

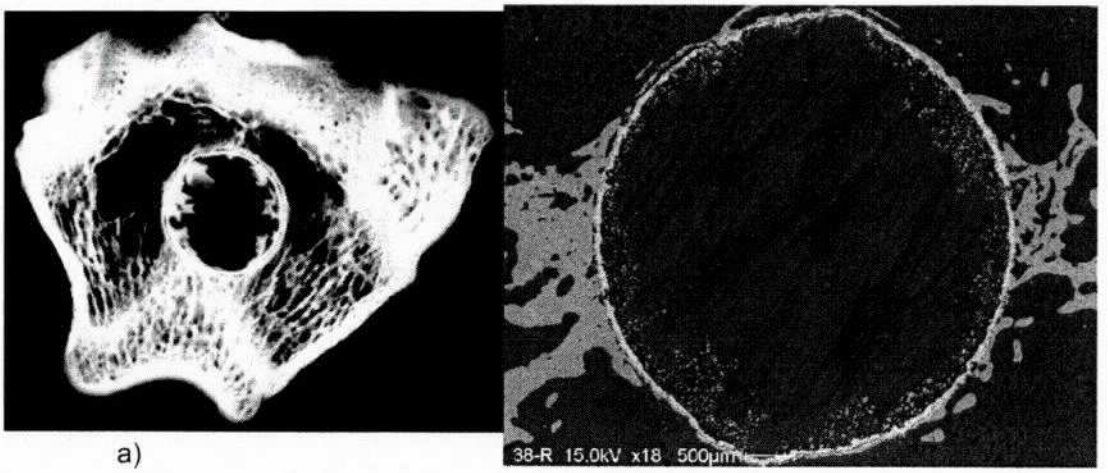

a)

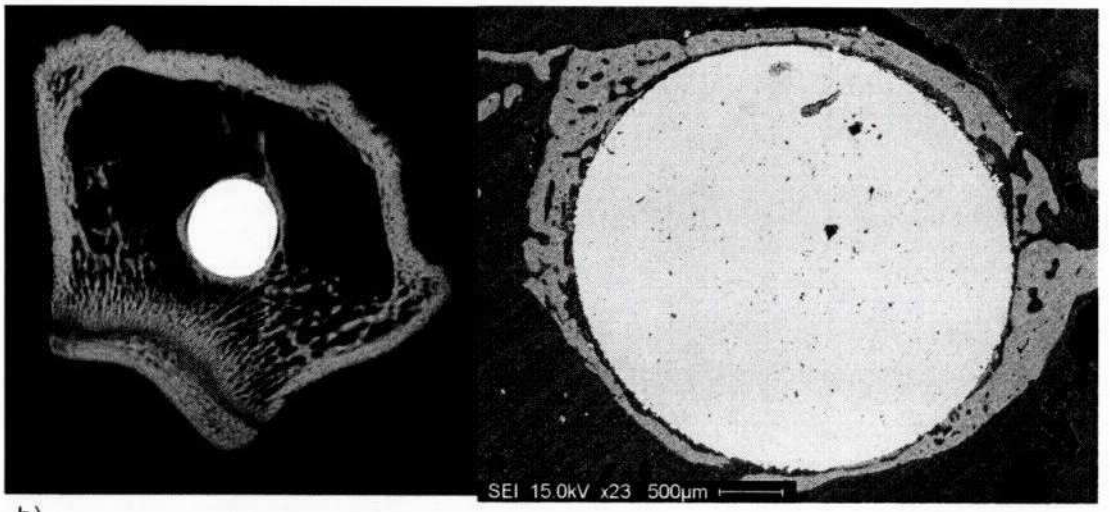

b)

Figure 12

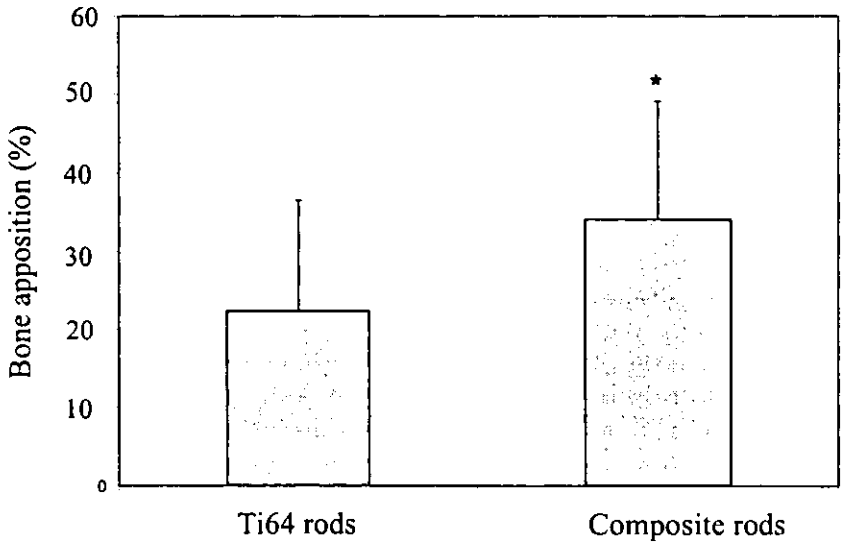

Table 1

Property	Ti-6Al-4V [22]	Polymer composite [14]
Elastic modulus (GPa)	114	12.2
Grit-blasting (μm)	6.38	6.38
HA coatings thickness (μm)	80	80
Ca/P ratio in HA	1.69 ± 0.04	1.69 ± 0.04
Crystaline index in HA (XRD)	0.60 ± 0.04	0.60 ± 0.04
Density (g/cm^3)	4.4	1.4